JGR Space Physics

RESEARCH ARTICLE
10.1029/2024JA032432

Observations of Relativistic Electron Precipitation Due To Combined Scattering of Whistler-Mode and EMIC Waves

M. Fraz Bashir[1], Anton Artemyev[1,2], Xiao-Jia Zhang[1,3], Vassilis Angelopoulos[1], Ethan Tsai[1], and Colin Wilkins[1]

[1]Earth, Planetary, and Space Sciences, University of California, Los Angeles, Los Angeles, CA, USA, [2]Space Research Institute, RAS, Moscow, Russia, [3]Department of Physics, University of Texas at Dallas, Richardson, TX, USA

Key Points:

- We report observations of energetic electron precipitation likely driven by concurrent whistle-mode and electromagnetic ion cyclotron (EMIC) waves
- The combined scattering of whistler-mode and EMIC waves leads to electron precipitation over a wide energy range of 50 keVs to a few MeVs
- This study highlights the potential nonlinear effects for explaining the observed energetic electron fluxes in the inner magnetosphere

Correspondence to:
M. F. Bashir,
frazbashir@epss.ucla.edu

Citation:
Bashir, M. F., Artemyev, A., Zhang, X.-J., Angelopoulos, V., Tsai, E., & Wilkins, C. (2024). Observations of relativistic electron precipitation due to combined scattering of whistler-mode and EMIC waves. *Journal of Geophysical Research: Space Physics*, *129*, e2024JA032432. https://doi.org/10.1029/2024JA032432

Received 8 JAN 2024
Accepted 14 APR 2024

Abstract The two most important wave modes responsible for energetic electron scattering to the Earth's ionosphere are electromagnetic ion cyclotron (EMIC) waves and whistler-mode waves. These wave modes operate in different energy ranges: whistler-mode waves are mostly effective in scattering sub-relativistic electrons, whereas EMIC waves predominately scatter relativistic electrons. In this study, we report the direct observations of energetic electron (from 50 keV to 2.5 MeV) scattering driven by the combined effect of whistler-mode and EMIC waves using ELFIN measurements. We analyze five events showing EMIC-driven relativistic electron precipitation accompanied by bursts of whistler-driven precipitation over a wide energy range. These events reveal an enhancement of relativistic electron precipitation by EMIC waves during intervals of whistler-mode precipitation compared to intervals of EMIC-only precipitation. We discuss a possible mechanism responsible for such precipitation. We suggest that below the minimum resonance energy (E_{min}) of EMIC waves, the whistler-mode wave may both scatter electrons into the loss-cone and accelerate them to higher energy (1–3 MeV). Electrons accelerated above E_{min} resonate with EMIC waves that, in turn, quickly scatter those electrons into the loss-cone. This enhances relativistic electron precipitation beyond what EMIC waves alone could achieve. We present theoretical support for this mechanism, along with observational evidence from the ELFIN mission. We discuss methodologies for further observational investigations of this combined whistler-mode and EMIC precipitation.

Plain Language Summary Energetic electron precipitation into the upper atmosphere is an important loss process of outer radiation belt fluxes. Whistler-mode and electromagnetic ion cyclotron (EMIC) waves are two of the most important wave modes responsible for energetic electron scattering to the Earth's ionosphere through wave-particle interaction. These wave modes typically drive losses of electrons in different energy ranges (above 1 MeV for EMIC waves and tens to hundreds of keV for whistler-mode waves), occurring in different spatial regions. We report the first observations of energetic electron scattering driven by the combined effect of whistler-mode and EMIC waves. Our results from equatorial and low-altitude observations, and a data-driven test particle simulation explain the wide energy range of electron precipitation from tens of keVs to a few MeVs due to the combined whistler-mode and EMIC waves effect and explain the unusually high intensity of relativistic electron precipitation at such times.

1. Introduction

Electromagnetic ion cyclotron (EMIC) and whistler-mode waves are two of the most important wave modes responsible for energetic electron scattering and precipitation from the Earth's radiation belts into the atmosphere (see reviews by Li & Hudson, 2019; Millan & Thorne, 2007; Thorne et al., 2021). EMIC waves are mostly responsible for the precipitation of relativistic (>1 MeV) electrons (e.g., Bashir & Ilie, 2018, 2021; Bashir et al., 2022b; Blum et al., 2015; Capannolo et al., 2018, 2022; Grach & Demekhov, 2020; Ni et al., 2015; Shprits et al., 2016, 2017; Usanova et al., 2014), whereas whistler-mode waves are very effective in precipitating sub-MeV electrons (see, e.g., reviews by Artemyev et al., 2016; Ni et al., 2016; Shprits et al., 2008; Thorne et al., 2021). Resonant scattering of relativistic (>1 MeV) electrons by whistler-mode waves is most effective at higher electron pitch-angles, which may not result in precipitation (e.g., Aryan et al., 2020; Horne et al., 2013). However, the combined effect of EMIC and whistler-mode waves may enable a rapid decrease of relativistic electron fluxes: whistler-mode waves scatter electrons at higher pitch-angles toward the lower pitch-angle range, where resonance with EMIC waves may quickly scatter these electrons into the loss-cone (e.g., Bashir et al., 2022a; Mourenas et al., 2016; Zhang et al., 2017). Therefore, relativistic electron losses by combined EMIC

and whistler-mode wave scattering are essential contributions to radiation belt dynamics (Drozdov et al., 2020). However, in contrast to electron resonance with EMIC waves providing only pitch-angle scattering (e.g., Summers & Thorne, 2003), resonance with whistler-mode waves can result in both pitch-angle and energy (acceleration) scattering (e.g., Glauert & Horne, 2005; Summers, 2005). If such acceleration is sufficiently fast and efficient (e.g., due to nonlinear resonant acceleration, see Omura et al. (2007) and Summers and Omura (2007)), EMIC waves may scatter the newly formed relativistic electron population, those accelerated by whistler-mode waves, into the loss cone (see discussion in Bashir et al., 2022a). Such precipitation may not require preexisting relativistic electron fluxes, and would not lead to the decrease of preexisting, for example, previously stably trapped, relativistic electron fluxes. Near-equatorial electron flux measurements usually cannot resolve the loss-cone (see rare exceptions in Kasahara et al., 2018a, 2018b), and the most promising approach to investigate precipitation mechanisms relies on the analysis of low-altitude measurements, which can easily separate pitch-angles of precipitating and trapped particles (see, e.g., Y. Chen et al., 2014; Li et al., 2013; Ni et al., 2014). In this study, we utilize low-altitude electron measurements from the ELFIN CubeSats, which provide energy and pitch-angle resolved electron distributions (Angelopoulos et al., 2020). More importantly for us, the energy resolution of ELFIN measurements is sufficiently high to distinguish precipitating patterns associated with energetic/relativistic electron scattering by EMIC waves and patterns associated with energetic electron scattering by whistler-mode waves (see discussion and examples in Angelopoulos et al., 2023). Therefore, by comparing ELFIN measurements during EMIC-only precipitation patterns and patterns showing the combined effect of whistler-mode and EMIC waves, we can unveil the efficiency of such a combined mechanism.

To provide a new population of relativistic electrons for subsequent EMIC-driven scattering, electron acceleration by whistler-mode waves should be sufficiently fast. The quasi-linear diffusion rates for average wave intensities show that pitch-angle scattering by EMIC waves is much faster than acceleration by whistler-mode waves (see, e.g., Glauert & Horne, 2005; Summers et al., 2007a). However, very intense whistler-mode waves may resonate with electrons nonlinearly and lead to the rapid formation of relativistic electrons via phase trapping (e.g., Bortnik et al., 2008; Demekhov et al., 2006, 2009; Vainchtein et al., 2018). Such acceleration is especially effective for phase trapping into the turning acceleration (see Bashir et al., 2022a; Hsieh & Omura, 2017; Hsieh et al., 2020; Omura et al., 2007; Summers & Omura, 2007). The rate of this acceleration mechanism may approach the rate of pitch-angle diffusion by EMIC waves, and thus can potentially provide rapid electron acceleration and subsequent losses. In contrast to the standard phase trapping acceleration associated with pitch-angle increase (e.g., Bortnik et al., 2008; Vainchtein et al., 2018), turning acceleration will lead to a pitch-angle decrease with energy increase (Omura et al., 2007), that is, accelerated particles are transported toward the loss-cone where EMIC waves will scatter them. We will first analyze four events of energetic electron precipitation observed by ELFIN. Additionally to the analysis of electron precipitation events with the combined effect of EMIC and whistler-mode waves, we will try to construct and test a simple scenario of enhanced electron precipitation via a combined effect of turning acceleration and EMIC-driven scattering. Although this scenario is based on well-known models of turning acceleration by intense whistler-mode waves and fast quasi-linear electron scattering by EMIC waves, the specific regime of such combined mechanism operation depends on multiple wave characteristics. To constrain ranges of these characteristics within some reasonable range, we use an event with near-equatorial THEMIS measurements (Angelopoulos, 2008) within the same MLT, L-shell sector where ELFIN observed signatures of EMIC and whistler-mode driven precipitations. This event provides some additional information about waves, but suffers from non-ideal timing of THEMIS and ELFIN observations.

We use low-altitude precipitation measurements from ELFIN (Angelopoulos et al., 2020) to investigate the effect of electron resonant acceleration by whistler-mode waves and the subsequent scattering into the atmosphere by EMIC waves. Section 2 provides an overview of four ELFIN events exhibiting clear signatures of the combined operation of whistler-mode and EMIC waves. Section 3 describes in detail one event benefiting from ELFIN in conjunction with equatorial wave measurements from THEMIS (Angelopoulos, 2008). Section 4 discusses possible mechanisms responsible for the enhanced precipitation of relativistic electrons in the simultaneous presence of EMIC and whistler-mode waves. Section 5 summarizes our main findings.

2. ELFIN Observations of Relativistic Electron Precipitation

We use data from the ELFIN-A CubeSat which is equipped with an energetic electron detector measuring 50 keV to 6 MeV electrons with an energy resolution of $\Delta E/E < 40\%$ and covering the full (180°) pitch angle twice over a

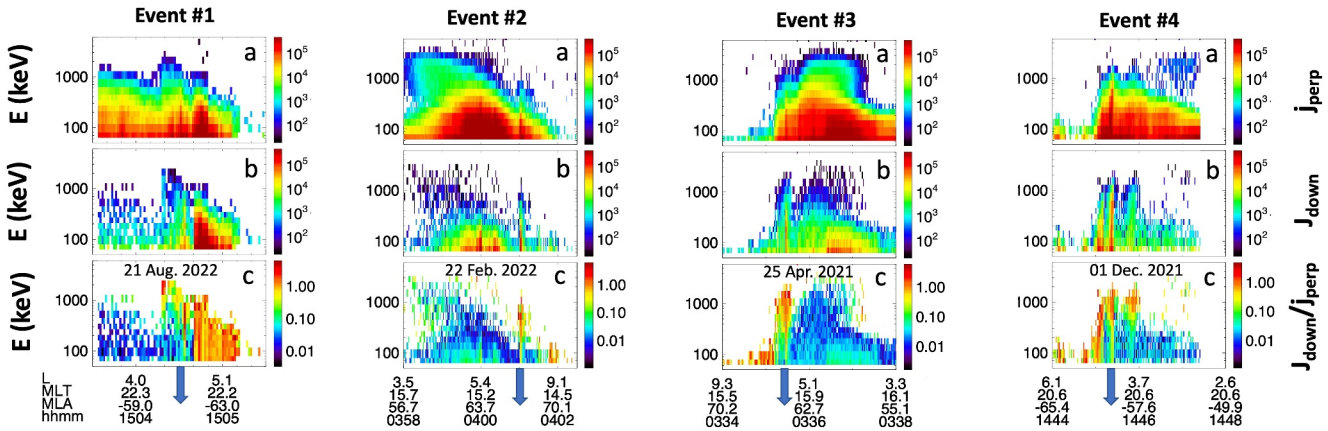

Figure 1. Four electron precipitation events observed by ELFIN: top panels (a) show locally trapped (i.e., outside the local loss cone, or near-perpendicular) electron fluxes j_{perp}; middle panels (b) depict precipitating or down-going fluxes (j_{down}); bottom panels (c) show precipitating (down-going)-to-perpendicular flux ratio (j_{down}/j_{perp}). The blue arrows mark the duration for the inserted panels in Figure 2a.

3 s spin period. Because of its high energy resolution, ELFIN can distinguish precipitation events driven by whistler-mode waves or by EMIC waves (X. An et al., 2022; Angelopoulos et al., 2023; Grach et al., 2022; Tsai et al., 2022; Zhang et al., 2022). Thus, we focus on putative combined precipitation events that demonstrate properties of both whistler-mode and EMIC wave-driven precipitation.

Figure 1 shows four ELFIN orbits with signatures of electron precipitation due to EMIC and whistler-mode waves. The typical minimum resonance energy for EMIC waves is ∼0.5–1 MeV (Kersten et al., 2014; Summers et al., 2007b), so only sub-intervals of relativistic precipitation without comparably strong sub-relativistic precipitation should be considered as evidence of EMIC-driven precipitation (see the detailed analysis of such events in Angelopoulos et al. (2023)). Typical minimum resonance energy for whistler-mode waves (low band chorus waves) is below 10 keV (Ni et al., 2012), whereas the scattering rate of electrons by whistler-mode waves decreases with increasing energy (Summers et al., 2007b). Thus, ELFIN observations of precipitation bursts with precipitating-to-trapped flux ratio maximizing at low energies should be interpreted as evidence of whistler-mode wave-driven precipitation (see the detailed analysis of such events in Tsai et al. (2022) and Zhang et al. (2022)). Middle panels of Figure 1 show that precipitation events contain both spin-scale bursts with EMIC-driven precipitation only (j_{down}/j_{perp} maximizing at relativistic energies) and bursts with combined whistler-mode and EMIC effects (j_{down}/j_{perp} is high over the entire energy range). Therefore, we may interpret these events as short-time-scale whistler-driven precipitation bursts embedded within large time-scale EMIC-driven precipitation. The scale difference is likely due to the different spatial scales of equatorial generation regions of EMIC waves (thousands of km, see Angelopoulos et al., 2023; Blum et al., 2016, 2017) and whistler-mode waves (hundreds of km, see Agapitov et al., 2017). Note that the precipitating flux levels during precipitation bursts are much higher than the background precipitating fluxes levels that is, indeed these observations allow us to compare the efficiency of EMIC-only versus EMIC and whistler-mode burst-driven precipitation with no contribution from background waves.

The top panels (bottom panels) of Figure 2 demonstrate precipitating (precipitating-to-perpendicular) electron spectra for several sub-intervals in each event: during EMIC-only precipitation patterns (with the precipitating-to-perpendicular flux ratio maximizing at relativistic energies), during EMIC and whistler-mode precipitation patterns (with the precipitating-to-trapped flux ratio maximizing at relativistic energies, but showing large values even at 50–100 keV energy channels), and background precipitation patterns before and after the precipitation as shown in the inserted panel. These spectra show that in the presence of whistler-mode waves, not only is precipitation of sub-relativistic electrons (<500 keV) enhanced but precipitation of relativistic electrons (likely scattered by EMIC waves) is also enhanced. This effect is best seen for event#4, where the presence of whistler-mode waves (detected by strong precipitating fluxes within <500 keV range) is associated with the enhancement of trapped fluxes and their precipitation for the energy range up to 2 MeV. Note that the trapped electron fluxes (those outside of the local loss-cone) at ELFIN correspond to the close vicinity (a few degrees) from the equatorial loss-cone, that is, these are almost field-aligned electrons likely scattered by EMICs to small pitch-angles, but not

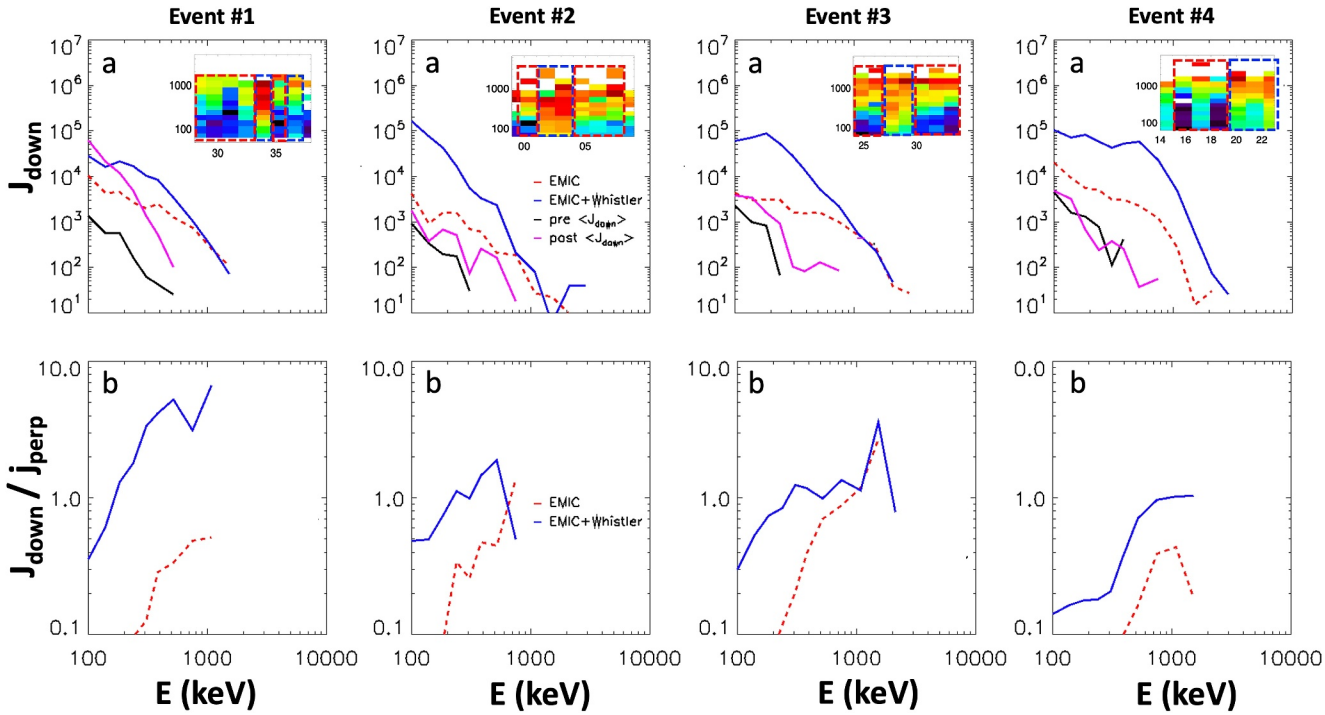

Figure 2. Top panels (a) show energy spectra of precipitating electrons during subintervals denoted by the arrow in Figure 1: inserts in this figure show relativistic and sub-relativistic electron precipitation bursts exhibiting electromagnetic ion cyclotron (EMIC) and whistler-mode (blue curve) and EMIC-only (magenta curve) signatures. These panels also include the average background fluxes before (pre $\langle j_{down} \rangle$) and after (post $\langle j_{down} \rangle$) each subinterval. The precipitating (down-going)-to-perpendicular flux ratio (j_{down}/j_{perp}) is depicted in the bottom panels (b). The inserted panels show j_{down}/j_{perp} from Figure 1 for the sub-intervals marked by the arrow (i.e., time in seconds after 15:04 UT (Event #1), 04:01 UT (Event #2), 03:35 UT (Event #3) and 14:45 UT (Event #4)). The blue and red dashed rectangular boxes inside inserted panels represent the spins related to EMIC + whistler and EMIC wave only respectively based on the criteria of $j_{down}/j_{perp} \geq 0.1$ for less than 100 keV energy.

yet precipitated. It is worth noting that the enhanced precipitation of relativistic electrons in the presence of whistler-mode waves is purely an effect of wave-particle interactions, as opposed to a result from the variability of the equatorially trapped fluxes: Figure 2 (bottom panels) shows the increase of precipitating-to-trapped flux ratio at relativistic energies, which can be attributed to enhanced electron scattering into the loss cone.

For all four events from Figures 1 and 2, we see the same pattern of combined EMIC and whistler-mode precipitation: long-lasting precipitation of relativistic electrons likely driven by EMICs interspersed with short (one spin) bursts of enhanced sub-relativistic electron precipitation likely driven by whistler-mode waves. It is exactly within such bursts that we observe enhanced relativistic precipitation. Such one-spin time scale of variations of ELFIN measurements is too small to be associated with spatial or temporal variations of EMIC waves (see discussion in Shumko et al., 2022), but can be explained by the concept of a burst of intense whistler-mode waves (see discussion in Zhang et al., 2023). Thus, we have an additional argument in support of the scenario of whistler-mode wave contribution to observed variations of relativistic electron precipitation.

In this study, we mostly focused on the scenario of electron acceleration by whistler-mode waves to the relativistic energies, and following scattering by EMIC waves. An alternative scenario could be that whistler-mode waves may scatter relativistic electrons and enhance precipitation on this energy range without direct contribution by EMIC waves (see Artemyev et al., 2021a; Lorentzen et al., 2001; Zhang et al., 2022, for the discussion on the possibility for intense whistler-mode waves to precipitation relativistic electrons). This scenario should assume even stronger precipitation at 50–100 keV range, where the efficiency of electron scattering by whistler-mode waves maximizes (see discussion in Y. Chen et al., 2014; Li et al., 2013; Ni et al., 2014, and references therein). However, Figure 1 shows an effective but still quite moderate precipitating-to-trapped flux ratio at 50–100 keV, suggesting that whistler-mode waves are not sufficiently intense to provide an enhancement of relativistic electron precipitation alone.

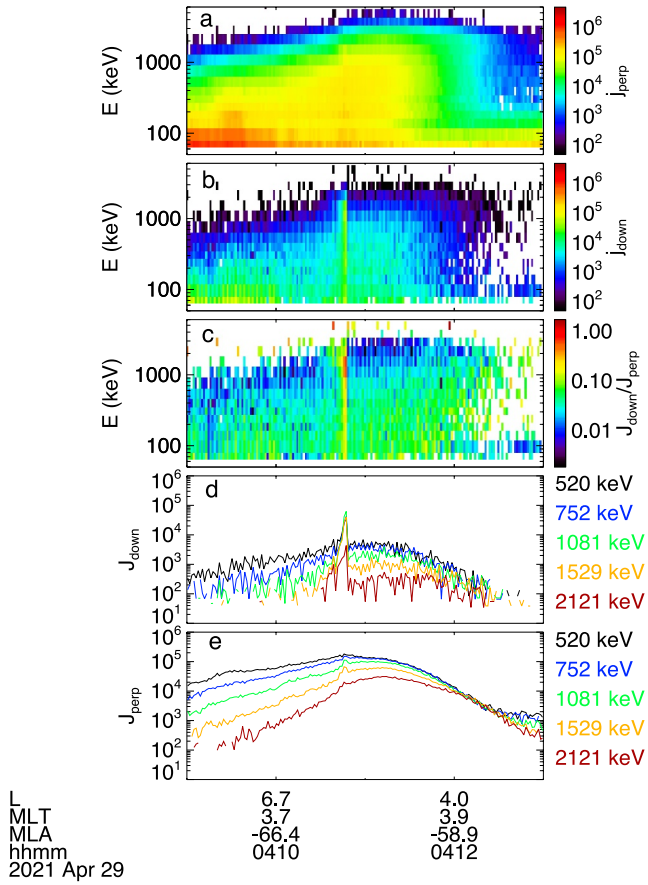

Figure 3. Overview of ELFIN-A observations: (a) locally trapped or perpendicular fluxes (j_{perp}), (b) precipitating or down-going fluxes (j_{down}), (c) precipitating-to-perpendicular flux ratio (j_{down}/j_{perp}), and 1D spectra (d) j_{down} and (e) j_{perp} at five energy channels (520–2,121 keV). L, MLT, and MLAT of ELFIN-A are marked at the bottom.

Another alternative scenario suggests that enhancement of relativistic and sub-relativistic electron precipitation may be associated with a strong enhancement of nonresonant electron scattering by EMIC waves (L. Chen et al., 2016), for example, due to increase of wave modulation to short wave-packets (see, e.g., X. An et al., 2022; Grach & Demekhov, 2020, 2023). This scenario is quite prospective, but requires additional mechanisms to explain the short-time-/small-spatial-scale variations of EMIC wave modulations.

3. Conjugate ELFIN and THEMIS Observations for Energetic Electron Precipitation Through the Combined Effects of Whistler and EMIC Waves

This section describes an additional event observed by ELFIN-A similar to those shown in Figures 1 and 2, but with near-equatorial wave measurements by THEMIS (See Figure 6). This event is in the post-midnight sector, not very typical for EMIC waves and relativistic electron precipitation (see statistics in Capannolo et al. (2022) and Yahnin et al. (2016, 2017)). In this region, the EMIC activity is largely associated with plasma sheet injections (Jun et al., 2019, 2021, and references theien). These plasma sheet injections may bring hot, anisotropic electrons responsible for whistler-mode generation (e.g., Fu et al., 2014; Tao et al., 2011).

Figure 3 shows the ELFIN-A measurements collected on 29 April 2021, at L-shell ~5 near the dawn sector of the southern hemisphere. At ~04:10:40 UT, precipitating (down-going) fluxes (J_{down}) of 300 keV to 2.5 MeV electrons suddenly increase with the highest precipitating to trapped flux ratio above 1 MeV. The locally trapped (near-perpendicular) electron fluxes (J_{perp}) show enhancement over a wide range of L-shells (4–6.5), exhibiting low precipitating to trapped flux ratio (J_{down}/J_{perp} is mostly less than 0.1) except for a few spins around 04:10:40 UT where this ratio can be greater than 0.5. The most intense burst of precipitation shows J_{down}/J_{perp} enhancement maximizing at relativistic energies ~1 MeV (the typical range of EMIC-driven precipitation), but extending down to 50 keV (the typical range of whistler-wave-driven precipitation). Note that the enhanced relativistic electron precipitation lasts longer than the enhancement of <500 keV precipitation (which only lasts for a single spin). This indicates a short whistler-mode burst embedded within a large-scale EMIC generation region (Figure 4).

Previous detailed investigations of EMIC wave driven (see analysis of events in, e.g., X. An et al., 2022; Capannolo et al., 2023; Grach et al., 2022) and whistler-mode wave driven (see analysis of events in, e.g., L. Chen et al., 2022; Zhang et al., 2022) electron precipitation events suggest that the several spin lasting precipitation of relativistic electron fluxes can be described by EMIC-only scattering, whereas a single-spin burst of precipitation should be provided by the combined effect of EMIC and whistler-mode waves.

During this event, ELFIN magnetically mapped close to the near-equatorial THEMIS-E spacecraft as shown in Figure 5 (Angelopoulos, 2008), which, at the time, was moving from lower L to higher L, observed the pertinent EMIC and whistler-mode waves and measured the properties of the cold plasma, and magnetic fields. We use magnetic field data from Flux Gate Magnetometer (FGM) (Auster et al., 2008). During fast mode, FGM measures waveforms at a time resolution of 1/16 s, sufficient to resolve the EMIC wave frequency range. Measurements of the THEMIS Search Coil Magnetometer (Le Contel et al., 2008) well cover the whistler-mode frequency range. The cold plasma density is inferred from the spacecraft potential (Nishimura et al., 2013) measured by THEMIS Electric Field Instrument (Bonnell et al., 2008).

Figure 6 shows that during this event, THEMIS-E observed whistler-mode waves around and outside of the plasmapause, identified as a strong plasma frequency (plasma density) gradient. At the plasmapause, THEMIS-E also observed He^+ band EMIC waves (field-aligned, left-hand polarized waves). The ratio of plasma to electron cyclotron frequency, $f_{pe}/f_{ce,eq}$, varies from ~20 to 25 across the plasmapause. Note that the projection of ELFIN to

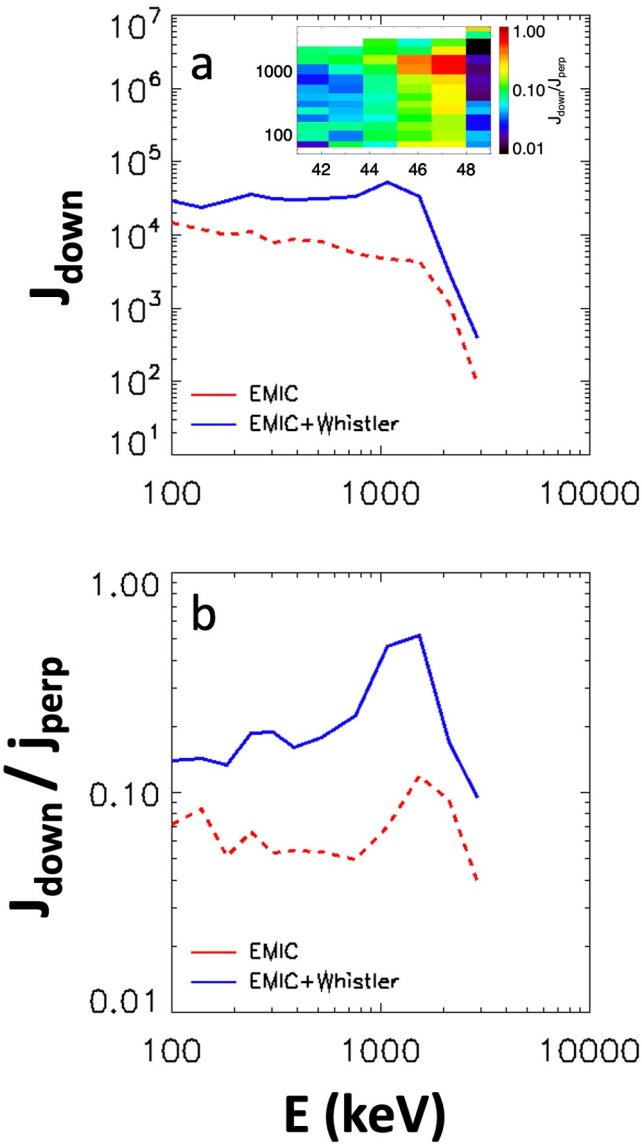

Figure 4. Overview of the observed fluxes by ELFIN-A depicting (a) the average precipitating or down-going fluxes (j_{down}), (b) precipitating-to-perpendicular flux ratio (j_{down}/j_{perp}) as a function of energy due to combined electromagnetic ion cyclotron (EMIC) and whistler-mode waves (solid-blue curve) and EMIC waves only (dashed-red curve) for the sub-interval (time in seconds after 04:10 UT) as shown by the inserted spectra of down-to-perpendicular flux ratio, which is in a similar format to panels (a) in Figure 2.

the equatorial plane is subject to uncertainties of empirical magnetic field models. Thus, this THEMIS-ELFIN conjunction is only approximate. ELFIN observations of relativistic electron precipitation burst and THEMIS observations of EMIC waves are within the $\Delta L = \pm 1$, ΔMLT = 2 of each other. These ranges are comparable to the spatial scale of the typical EMIC wave source region (Blum et al., 2016, 2017), whereas an ~40 min time difference between THEMIS and ELFIN observations is within the lifetime of EMIC wave source region (Blum et al., 2020; Engebretson et al., 2015). Therefore, we may suggest that ELFIN observations of relativistic electron precipitation are provided by EMIC waves having similar characteristics to waves observed by THEMIS *E*. However, we should note that the EMIC burst is observed by THEMIS *E* only, whereas A and *D* located $\pm 1.5 R_E$ away from *E* do not detect these EMIC bursts. Thus, we cannot exclude the possibility of a small-scale EMIC source region (e.g., Frey et al., 2004). But ELFIN observations of relativistic electron precipitation without ~50 keV precipitation (two spins before the main precipitation burst, see the inserted panel in Figure 1c) confirm that there was scattering by equatorial EMIC waves, which may relate to THEMIS-E observations.

All three THEMIS probes observe whistler mode waves during the entire ~2 hr interval at ΔMLT ~ 2. Therefore, we deal with a long-lived and large-scale spatial domain filled by whistler-mode source regions (note that individual whistler-mode bursts are separated in THEMIS spectra). ELFIN observations of weak but large-scale (seen almost for the entire ELFIN orbit) electron precipitation within <200 keV energy range suggest the near-equatorial electron scattering and precipitation by these whistler-mode wave activity. Nearby the plasmapause such not-very intense whistler-mode waves may be ducted (see R. Chen et al., 2021; Streltsov & Bengtson, 2020, and references therein), and such ducting would suppress wave Landau damping and support wave interaction with relativistic electrons at middle latitudes (see discussions in L. Chen et al., 2021, 2022). Thus, the overlapping of the EMIC wave source region, observed within the plasmapause, and region of potential whistler-mode wave ducting can explain the strong electron precipitation burst embedded into the large-scale EMIC-only precipitation.

4. Discussion

Figures 1 and 3 show that the presence of whistler-mode waves may enhance the precipitation of relativistic electrons. One possible mechanism of such enhancement is that intense whistler-mode waves drive electron acceleration (e.g., turning acceleration, see Omura et al., 2007; Summers & Omura, 2007), and the accelerated electrons supplement the population that is to be scattered by EMIC waves (Bashir et al., 2022a). In order to verify this scenario, we perform simple test particle simulations. The simulations are based on Hamiltonian equations for a monochromatic wave (see Artemyev et al., 2021b; Vainchtein et al., 2018), and this simplification (constant wave frequency) may reduce the efficiency of wave-particle resonant interactions (see discussion of frequency drift contribution in Demekhov et al. (2006), Hiraga and Omura (2020), and Katoh and Omura (2007)). Results of our test particle simulations can qualitatively imply that the proposed scenario of electron acceleration by whistler-mode waves and the following scattering by EMIC waves may work within a reasonable range of the system (wave) characteristics. More rigorous comparisons are necessary to quantify the efficiency of such a combined mechanism. Such simulations may not be performed within the quasi-linear approach, because the key element of the proposed scenario is the electron turning acceleration, the nonlinear resonant effect (Omura et al., 2007). Thus, further investigations of this scenario should include the nonlinear resonant effects. In previous studies, such simulations were developed for whistler-mode waves only (Hsieh &

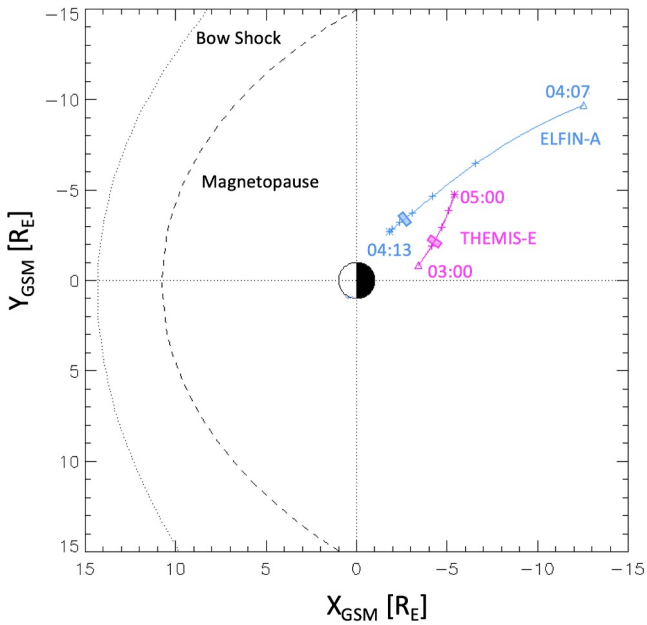

Figure 5. Overview of the spacecraft trajectories of THEMIS-E (magenta line) and close conjunction with ELFIN-A (blue line) with + symbol represents the time step of 30 min for THEMIS and 1 min for ELFIN respectively. The location of electromagnetic ion cyclotron and Whistler waves observed by THEMIS is represented by a small blue rectangular box and precipitation by ELFIN via a small magenta rectangular box The location of model Bow shock (black dotted) and magnetopause (black dashed) is also shown. The Tsyganenko (T96) magnetic field is used for calculations.

Omura, 2023; Hsieh et al., 2022; Omura et al., 2015; Vainchtein et al., 2018) or for EMIC waves only (Zheng et al., 2019).

The cyclotron resonance of electrons and whistler/EMIC waves is described by the wave field $\sqrt{2I_x\Omega_0/m_ec^2}B_w\Lambda(\lambda)\Phi(\phi)\sin(\phi\pm\theta)$, where I_x and θ are conjugated magnetic moment and gyrophase, B_w is the constant wave magnitude, $\Lambda(\lambda)$ describes the wave intensity distribution along magnetic field lines, $\Phi(\phi)$ describes wave field modulation (and we indeed use moderate modulation), ϕ is the wave phase given by $\dot{\phi}=-\omega+k(\lambda)p_{\|}/m_e\gamma$ where $k(\lambda)$ is the wave number from the wave dispersion relation for given wave frequency ω, $p_{\|}/m_e\gamma$ is the electron parallel velocity equal to the ratio of momentum and Lorentz factor.

We model the precipitation event in Figure 3, for which we have near-equatorial observations of waves (see Figure 6). For the whistler wave, we use the observed frequency $f_{wh}/f_{ce,eq}=0.3$ and 0.4, with an amplitude at $B_{w,wh}=500$ pT $\cdot\ \Lambda(\lambda)$. Function $\Lambda(\lambda)$ describes the latitudinal profile of the whistler wave intensity (amplitude): $\Lambda(\lambda)=0.5\cdot\ (1+\tanh(\lambda/\delta\lambda_1))\ \exp\left(-(\lambda/\delta\lambda_2)^2\right)$ and $\delta\lambda_{1,2}=1°, 40°$ (e.g., we assume wave generation at the equator and damping at high latitudes, see details of this empirical wave model in Agapitov et al., 2018). For the ducted whistler case, we have used $\Lambda(\lambda)\rightarrow 1$. We also include wave field modulation by assuming that whistler-mode waves propagate in wave packets: $B_{w,wh}\rightarrow B_{w,wh}\cdot\Phi(\phi)$ with $\Phi(\phi)=\exp(-0.25\cdot(\sin(\phi/(2\pi l))^2))$, where ϕ is the wave phase and $l=300$ determines the wave-packet size (we use the longest wave packets from observations, see statistics in Zhang et al. (2019, 2021)). Function $\Phi(\phi)$ describes the wave-packet envelop that propagates with the wave phase speed, $\omega/k(\lambda)$ (note that we assume monochromatic waves). For realistic wave-packets, the propagation speed is the group speed $v_g=\partial\omega/\partial k$, which differs from the phase speed ω/k. Such packets will evolve over time because the different wave harmonics contributing to the packet will propagate at different speeds (see Furuya et al., 2008; Tao et al., 2012). Our simplified consideration of the wave-packet propagation with the phase speed can be interpreted as the absence of wave-packet evolution: instead of the sum of multiple plane waves, we model wave-packet as an amplitude modulation of the monochromatic wave. Although this simplified model excludes effects of wave-packet evolution (that can be quite important for nonlinear resonant interactions, see discussion in Z. An et al. (2022) and Tao et al. (2012, 2013)), it catches the main effect: the difference between wave-packet envelop speed and resonant electron speed, $\left(\omega-2\pi f_{ce}(\lambda)\right)/k(\lambda)$, limits the electron trapping time. Note, however, we do not include wave phase decoherence at the wave-packet edges (see discussion in Z. An et al. (2022) and Zhang et al. (2020a)), and thus our simulation does not exclude multiple trapping effects into the wave-packet train (Hiraga & Omura, 2020).

For the He^+ band EMIC wave, we use the most intense wave from observations, with an amplitude of $B_{w,\mathrm{EMIC}}=500$ pT, at a fixed frequency $f_{\mathrm{EMIC}}/f_{cp,eq}=0.2$. Plasma composition is assumed to be 20% helium and 80% cold protons (Lee & Angelopoulos, 2014; Lee et al., 2012), and latitudinal distribution of EMIC waves as $B_{w,\mathrm{EMIC}}\rightarrow B_{w,\mathrm{EMIC}}\cdot\Lambda(\lambda)$ with $\Lambda(\lambda)=0.5(\tanh(\lambda/\delta\lambda_1)-\tanh((\lambda-\delta\lambda_2)/\delta\lambda_1))$ with $\delta\lambda_{1,2}=1°, 15°$, that is, there is no EMIC wave around and above the helium resonance latitude that is around ~25° for the selected wave frequency. For this study, we used the field-aligned cold plasma dispersion relation for both whistler and EMIC waves (Stix, 1962), with $f_{pe}/f_{ce,eq}=20$, and $L=4.5$. The time is normalized to a typical scale $R/c\sim 0.1$ s as $R=4.5$ R_E, where R_E is the radius of the Earth and c is the speed of light.

Figure 7 shows two loss mechanisms of energetic electrons with initial pitch-angles that are not in resonance with EMIC waves: (a) electrons directly scattered into the loss-cone by whistler-mode waves (blue trajectory) or (b) electrons phase trapped and accelerated by whistler-mode waves to energies sufficiently high for resonance with EMIC waves, and then scattered into loss-cone by EMIC waves (magenta trajectory). Importantly, the electron acceleration via phase trapping takes less than the electron bounce period, and this explains the bursty nature of

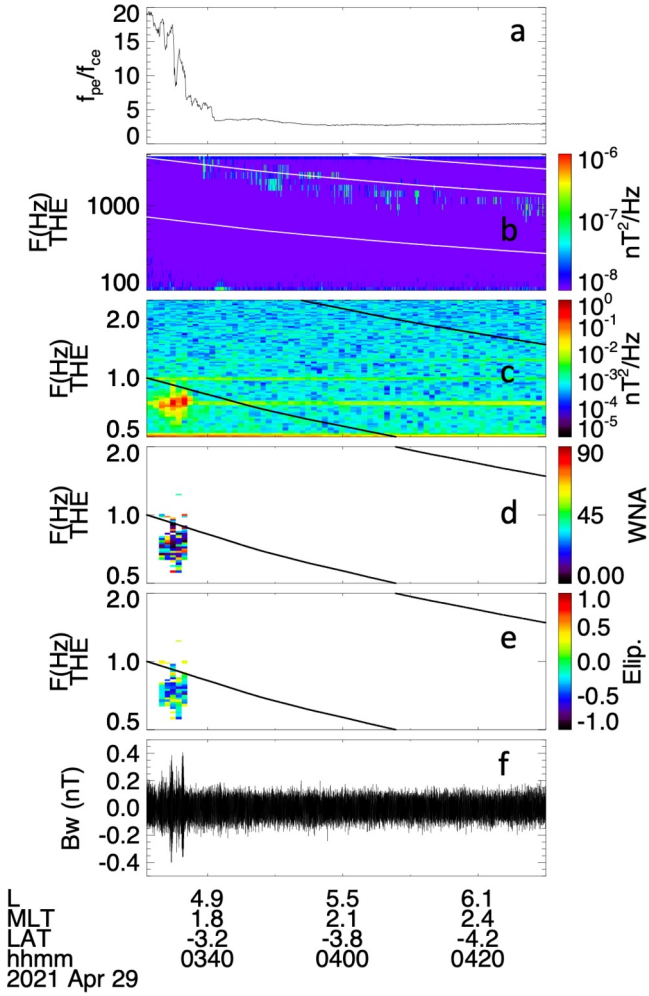

Figure 6. Overview of THEMIS-E observations: (a) f_{pe}/f_{ce} ratio, (b) whistler wave spectra, (c) electromagnetic ion cyclotron (EMIC) wave spectrum with its (d) ellipticity and (e) wave normal angle (WNA). Horizontal white lines in the whistler wave spectra represent f_{ce}, 0.5 f_{ce}, and 0.1 f_{ce}, respectively, whereas horizontal black lines in the next three panels represent f_{cp}, and f_{cHe}, respectively. The bottom panel (f) shows the EMIC wave packets. L, MLT, and LAT from TH-E are shown at the bottom.

observed electron precipitations detected by ELFIN on a spin time scale (see Figures 1 and 3). Resonance with whistler-mode waves moves electrons along the resonance curves (Summers et al., 1998), and thus we are interested in those that will cross the region (above the $E_{\min}$ shown by a thick red curve) of electron resonant interaction with EMIC waves (the latter interactions, primarily resulting in pitch-angle scattering, occur along the thin horizontal red lines). For moderate electron energies, phase trapping results in energy and pitch-angle increase (e.g., Bortnik et al., 2008; Vainchtein et al., 2018), and thus resonance curves move away from the loss-cone. However, when the electron energy reaches $\gamma > f_{ce}/f$, its pitch-angle starts to decrease during the phase trapping (so-called turning acceleration Bashir et al., 2022a; Omura et al., 2007). This effect bends the resonance curves back toward smaller pitch-angles. It thus allows the accelerated electron to escape from the trapping at an energy and pitch-angle where resonance with EMIC waves can occur. Figure 7 shows that such a double resonance effect (trapping acceleration by whistler-mode waves followed by scattering into loss-cone by EMIC waves) covers an energy range where strong precipitation was observed in our event (Figure 3).

However, certain wave characteristics (e.g., the latitudinal extent) cannot be derived from single-spacecraft observations. Therefore, to verify the applicability of the double resonance precipitation mechanism (acceleration by whistler-mode waves and scattering into the loss-cone by EMIC waves), we perform a series of simulations with different wave parameters. As shown in Figure 8, change of wave propagation mode (ducted with $B_w \approx const$ and non-ducted with B_w decreases to zero above 40°), wave frequency, and wave packet sizes may only change the final energy range of electron precipitation, but do not switch off the double resonance mechanism. The simulation results in time units are also (shown in Figure 9).

The model results suggest the following scenario for the formation of the observed electron precipitation spectrum: The source size of EMIC waves is usually sufficiently large (Blum et al., 2016, 2017) to provide relativistic electron precipitation within an $\sim 1 R_E$ region near the equator (Capannolo et al., 2019), which corresponds to several spins of ELFIN observations at low altitudes (see several examples of ELFIN observed EMIC-driven precipitation in, e.g., X. An et al., 2022; Angelopoulos et al., 2023; Grach et al., 2021). Therefore, the relativistic electron precipitation (without strong electron precipitation at <100 keV) within 04:10:35–04:10:50 UT should be attributed to EMIC waves. At the beginning of this subinterval, there is no strong sub-MeV precipitation (see j_{down}/j_{perp} in Figure 3) which we assert is indicative of an absence of strong whistler-mode waves. We interpret the following burst of <1 MeV precipitation around 04:10:45 UT as due to a whistler-mode wave burst (the short duration of the precipitation burst should be attributed to the small scale of whistler-mode wave source region near the equator, see Agapitov et al., 2017). This whistler-mode wave burst is sufficiently strong to provide electron acceleration, and thus efficiently increase >1 MeV electron fluxes that are further precipitated by EMIC waves (see an increase of j_{perp} associated with j_{down} increase in Figure 3). However, we shall caution that due to large uncertainties of ELFIN/THEMIS mapping and the time/spatial separation of precipitation events and THEMIS wave measurements, this interpretation is presently a reasonable hypothesis supported by the limited data set examined, and needs to be confirmed by further multi-point and statistical analysis in the future. Moreover, we used a rather simplified wave model that may not describe all aspects of wave-particle nonlinear resonances. Therefore, results shown in Figures 7–9 should be considered as an indication that the combined whistler-mode and EMIC resonant interactions with electrons may explain the enhanced relativistic electron precipitation observed in Figures 1 and 3; but more sophisticated and detailed simulations are needed to confirm this scenario and assess the overall efficiency of the proposed combined precipitation mechanism.

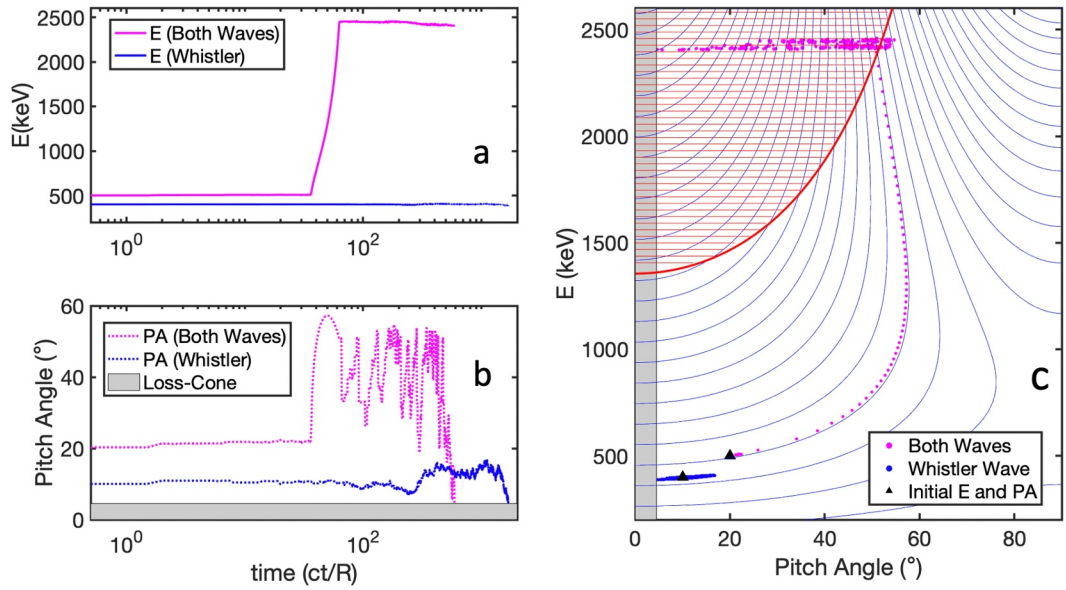

Figure 7. Illustrative electron trajectories from our simulations. Panels (a) and (b) depict the temporal (in units of ct/LR_E) evolution of the electron's energy and pitch angle for whistler-mode waves only (blue curve) and for the combined effect (magenta curve) of whistler-mode and electromagnetic ion cyclotron (EMIC) waves. The loss-cone (assumed to be 4.5°) is shaded in gray in Panel (b). Panel (c) shows the same trajectories on an energy, pitch-angle plane, with resonance curves for whistler-mode (blue curves) and EMIC (red lines) waves overlaid, and the range of EMIC resonance energies is shown by a thick red curve. The blue dots show electron trajectory (starting at an initial energy of 400 keV and an equatorial pitch angle of 10°, represented by the triangle) directly scattered by whistler waves into loss-cone; the other electron trajectory (magenta dots), with an initial energy of 500 keV and an equatorial pitch angle of 20°, show that the electron gets accelerated by whistler waves and then quickly scattered into loss-cone by EMIC waves.

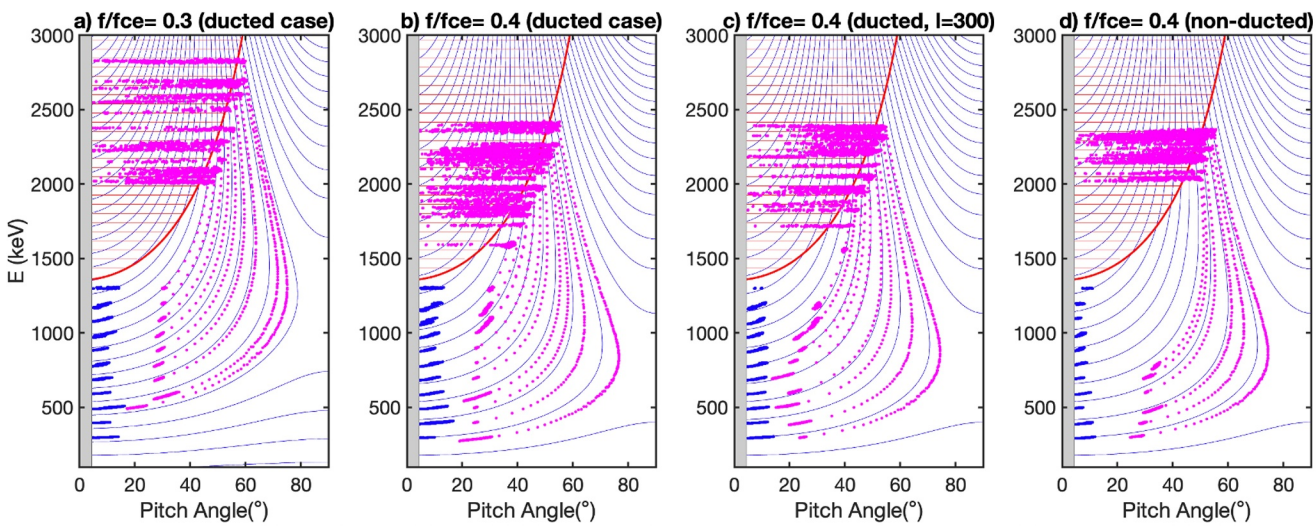

Figure 8. The temporal evolution of electron trajectories with different initial energies (300 keV to 1 MeV) and pitch angles (7°–65°) are depicted in energy and pitch-angle space for $f_{wh}/f_{ce,eq} = 0.3$ in panel (a) and $f_{wh}/f_{ce,eq} = 0.4$ in panels (b), (c), and (d). Panels (a) and (b) show the results for the ducted whistler case, (c) for the ducted case with long but finite wave-packets ($l = 300$) (Zhang et al., 2020b) and (d) for the non-ducted case. Magenta trajectories show those first accelerated to relativistic energies by whistlers and then scattered by electromagnetic ion cyclotron (EMIC) waves, whereas blue ones show those only scattered by whistler waves. The overplotted blue and red lines are theoretically calculated and the thick red curve marks the minimum resonant energy ($E_{\min}$) with EMIC waves. The gray vertical shade represents the loss cone which is assumed to be 4.5° in our simulations.

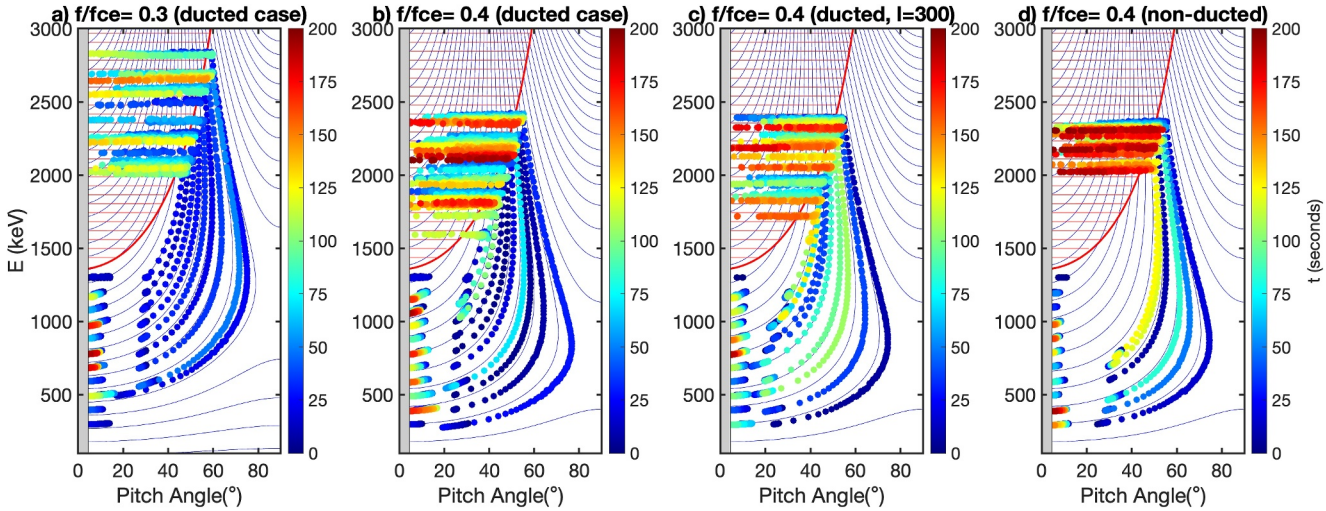

Figure 9. Same as Figure 8 with the addition of the simulation time of each trajectory in seconds.

5. Conclusions

This paper reports the observation of relativistic electron precipitation driven by the scattering of EMIC waves with the effect of precipitation enhancement by concurrent whistler-mode waves. For five events, ELFIN observed electron precipitation at 300 keV to 2.5 MeV, and precipitating fluxes which were higher during subintervals containing both EMIC and whistler-driven precipitation, compared to subintervals of EMIC-driven precipitation alone. We propose the scenario of electron acceleration (via the nonlinear resonant acceleration, e.g., phase trapping and turning acceleration) by whistler-mode waves up to relativistic energies and subsequent scattering of this accelerated electron population by EMIC waves. Simplified test particle simulations confirm that this scenario indeed can work. Our results suggest that nonlinear resonant acceleration (Omura et al., 2007, 2015) may significantly contribute to electron precipitation events observed at low altitudes.

Data Availability Statement

Fluxes measured by ELFIN are available in ELFIN data archive https://data.elfin.ucla.edu/ in CDF format.

THEMIS data is available at http://themis.ssl.berkeley.edu/data/themis. Data analysis was done using SPEDAS V4.1 (Angelopoulos et al., 2019). The software can be downloaded from http://spedas.org/wiki/index.php?title=Downloads_and_Installation.

Acknowledgments

A.V.A, X.-J.Z., and M.F.B. acknowledge support from the NASA Grants 80NSSC20K1270, 80NSSC23K0403, 80NSSC24K0138, and 80NSSC19K0844. X.-J. Z. acknowledges support from the NSF Grant 2329897. V.A. acknowledges support by NSF Grants AGS-1242918, and AGS-2019950. We are grateful to NASA's CubeSat Launch Initiative for ELFIN's successful launch in the desired orbits. We acknowledge the early support of the ELFIN project by the AFOSR, under its University Nanosat Program, UNP-8 project, contract FA9453-12-D-0285, and by the California Space Grant program. We acknowledge the critical contributions of numerous volunteer ELFIN team student members. We also acknowledge NASA contract NAS5-02099 for use of data from the THEMIS mission. We thank K. H. Glassmeier, U. Auster, and W. Baumjohann for the use of FGM data provided under the lead of the Technical University of Braunschweig and with financial support through the German Ministry for Economy and Technology and the German Aerospace Center (DLR) under contract 50 OC 0302.

References

Agapitov, O. V., Blum, L. W., Mozer, F. S., Bonnell, J. W., & Wygant, J. (2017). Chorus whistler wave source scales as determined from multipoint Van Allen Probe measurements. *Geophysical Research Letters*, *44*(6), 2634–2642. https://doi.org/10.1002/2017GL072701

Agapitov, O. V., Mourenas, D., Artemyev, A. V., Mozer, F. S., Hospodarsky, G., Bonnell, J., & Krasnoselskikh, V. (2018). Synthetic empirical chorus wave model from combined Van Allen Probes and cluster statistics. *Journal of Geophysical Research: Space Physics*, *123*(1), 297–314. https://doi.org/10.1002/2017JA024843

An, X., Artemyev, A., Angelopoulos, V., Zhang, X., Mourenas, D., & Bortnik, J. (2022). Nonresonant scattering of relativistic electrons by electromagnetic ion cyclotron waves in Earth's radiation belts. *Physical Review Letters*, *129*(13), 135101. https://doi.org/10.1103/PhysRevLett.129.135101

An, Z., Wu, Y., & Tao, X. (2022). Electron dynamics in a chorus wave field generated from particle-in-cell simulations. *Geophysical Research Letters*, *49*(3), e97778. https://doi.org/10.1029/2022GL097778

Angelopoulos, V. (2008). The THEMIS mission. *Space Science Reviews*, *141*(1–4), 5–34. https://doi.org/10.1007/s11214-008-9336-1

Angelopoulos, V., Cruce, P., Drozdov, A., Grimes, E. W., Hatzigeorgiu, N., King, D. A., et al. (2019). The Space physics environment Data Analysis System (SPEDAS). *Space Science Reviews*, *215*(1), 9. https://doi.org/10.1007/s11214-018-0576-4

Angelopoulos, V., Tsai, E., Bingley, L., Shaffer, C., Turner, D. L., Runov, A., et al. (2020). The ELFIN mission. *Space Science Reviews*, *216*(5), 103. https://doi.org/10.1007/s11214-020-00721-7

Angelopoulos, V., Zhang, X. J., Artemyev, A. V., Mourenas, D., Tsai, E., Wilkins, C., et al. (2023). Energetic electron precipitation driven by electromagnetic ion cyclotron waves from Elfin's low altitude perspective. *Space Science Reviews*, *219*(5), 37. https://doi.org/10.1007/s11214-023-00984-w

Artemyev, A. V., Agapitov, O., Mourenas, D., Krasnoselskikh, V., Shastun, V., & Mozer, F. (2016). Oblique whistler-mode waves in the Earth's inner magnetosphere: Energy distribution, origins, and role in radiation belt dynamics. *Space Science Reviews*, *200*(1–4), 261–355. https://doi.org/10.1007/s11214-016-0252-5

Artemyev, A. V., Demekhov, A. G., Zhang, X. J., Angelopoulos, V., Mourenas, D., Fedorenko, Y. V., et al. (2021a). Role of ducting in relativistic electron loss by whistler-mode wave scattering. *Journal of Geophysical Research: Space Physics*, *126*(11), e29851. https://doi.org/10.1029/2021JA029851

Artemyev, A. V., Neishtadt, A. I., Vasiliev, A. A., Zhang, X.-J., Mourenas, D., & Vainchtein, D. (2021b). Long-term dynamics driven by resonant wave-particle interactions: From Hamiltonian resonance theory to phase space mapping. *Journal of Plasma Physics*, *87*(2), 835870201. https://doi.org/10.1017/S0022377821000246

Aryan, H., Agapitov, O. V., Artemyev, A., Mourenas, D., Balikhin, M. A., Boynton, R., & Bortnik, J. (2020). Outer radiation belt electron lifetime model based on combined Van Allen Probes and cluster VLF measurements. *Journal of Geophysical Research: Space Physics*, *125*(8), e28018. https://doi.org/10.1029/2020JA028018

Auster, H. U., Glassmeier, K. H., Magnes, W., Aydogar, O., Baumjohann, W., Constantinescu, D., et al. (2008). The THEMIS fluxgate magnetometer. *Space Science Reviews*, *141*(1–4), 235–264. https://doi.org/10.1007/s11214-008-9365-9

Bashir, M. F., Artemyev, A., Zhang, X.-J., & Angelopoulos, V. (2022a). Energetic electron precipitation driven by the combined effect of ULF, EMIC, and whistler waves. *Journal of Geophysical Research: Space Physics*, *127*(1), e2021JA029871. https://doi.org/10.1029/2021JA029871

Bashir, M. F., Artemyev, A., Zhang, X.-J., & Angelopoulos, V. (2022b). Hot plasma effects on electron resonant scattering by electromagnetic ion cyclotron waves. *Geophysical Research Letters*, *49*(11), e2022GL099229. https://doi.org/10.1029/2022GL099229

Bashir, M. F., & Ilie, R. (2018). A new N^+ band of electromagnetic ion cyclotron waves in multi-ion cold plasmas. *Geophysical Research Letters*, *45*(19), 10150–10159. https://doi.org/10.1029/2018GL080280

Bashir, M. F., & Ilie, R. (2021). The first observation of N^+ electromagnetic ion cyclotron waves. *Journal of Geophysical Research: Space Physics*, *126*(3), e2020JA028716. https://doi.org/10.1029/2020JA028716

Blum, L. W., Agapitov, O., Bonnell, J. W., Kletzing, C., & Wygant, J. (2016). EMIC wave spatial and coherence scales as determined from multipoint Van Allen Probe measurements. *Geophysical Research Letters*, *43*(10), 4799–4807. https://doi.org/10.1002/2016GL068799

Blum, L. W., Bonnell, J. W., Agapitov, O., Paulson, K., & Kletzing, C. (2017). EMIC wave scale size in the inner magnetosphere: Observations from the dual Van Allen Probes. *Geophysical Research Letters*, *44*(3), 1227–1233. https://doi.org/10.1002/2016GL072316

Blum, L. W., Halford, A., Millan, R., Bonnell, J. W., Goldstein, J., Usanova, M., et al. (2015). Observations of coincident EMIC wave activity and duskside energetic electron precipitation on 18–19 January 2013. *Geophysical Research Letters*, *42*(14), 5727–5735. https://doi.org/10.1002/2015GL065245

Blum, L. W., Remya, B., Denton, M. H., & Schiller, Q. (2020). Persistent EMIC wave activity across the nightside inner magnetosphere. *Geophysical Research Letters*, *47*(6), e87009. https://doi.org/10.1029/2020GL087009

Bonnell, J. W., Mozer, F. S., Delory, G. T., Hull, A. J., Ergun, R. E., Cully, C. M., et al. (2008). The Electric Field Instrument (EFI) for THEMIS. *Space Science Reviews*, *141*(1–4), 303–341. https://doi.org/10.1007/s11214-008-9469-2

Bortnik, J., Thorne, R. M., & Inan, U. S. (2008). Nonlinear interaction of energetic electrons with large amplitude chorus. *Geophysical Research Letters*, *35*(21), 21102. https://doi.org/10.1029/2008GL035500

Capannolo, L., Li, W., Ma, Q., Qin, M., Shen, X. C., Angelopoulos, V., et al. (2023). Electron precipitation observed by ELFIN using proton precipitation as a Proxy for Electromagnetic Ion Cyclotron (EMIC) waves. *Geophysical Research Letters*, *50*(21), e2023GL103519. https://doi.org/10.1029/2023GL103519

Capannolo, L., Li, W., Ma, Q., Shen, X. C., Zhang, X. J., Redmon, R. J., et al. (2019). Energetic electron precipitation: Multievent analysis of its spatial extent during EMIC wave activity. *Journal of Geophysical Research: Space Physics*, *124*(4), 2466–2483. https://doi.org/10.1029/2018JA026291

Capannolo, L., Li, W., Ma, Q., Zhang, X.-J., Redmon, R. J., Rodriguez, J. V., et al. (2018). Understanding the driver of energetic electron precipitation using coordinated multisatellite measurements. *Geophysical Research Letters*, *45*(14), 6755–6765. https://doi.org/10.1029/2018GL078604

Capannolo, L., Li, W., Millan, R., Smith, D., Sivadas, N., Sample, J., & Shekhar, S. (2022). Relativistic electron precipitation near midnight: Drivers, distribution, and properties. *Journal of Geophysical Research: Space Physics*, *127*(1), e2021JA030111. https://doi.org/10.1029/2021JA030111

Chen, L., Thorne, R. M., Bortnik, J., & Zhang, X.-J. (2016). Nonresonant interactions of electromagnetic ion cyclotron waves with relativistic electrons. *Journal of Geophysical Research*, *121*(10), 9913–9925. https://doi.org/10.1002/2016JA022813

Chen, L., Zhang, X.-J., Artemyev, A., Angelopoulos, V., Tsai, E., Wilkins, C., & Horne, R. B. (2022). Ducted chorus waves cause sub-relativistic and relativistic electron microbursts. *Geophysical Research Letters*, *49*(5), e97559. https://doi.org/10.1029/2021GL097559

Chen, L., Zhang, X.-J., Artemyev, A., Zheng, L., Xia, Z., Breneman, A. W., & Horne, R. B. (2021). Electron microbursts induced by nonducted chorus waves. *Frontiers in Astronomy and Space Sciences*, *8*, 163. https://doi.org/10.3389/fspas.2021.745927

Chen, R., Gao, X., Lu, Q., Tsurutani, B. T., & Wang, S. (2021). Observational evidence for whistler mode waves guided/ducted by the inner and outer edges of the plasmapause. *Geophysical Research Letters*, *48*(6), e92652. https://doi.org/10.1029/2021GL092652

Chen, Y., Reeves, G. D., Friedel, R. H. W., & Cunningham, G. S. (2014). Global time-dependent chorus maps from low-Earth-orbit electron precipitation and Van Allen Probes data. *Geophysical Research Letters*, *41*(3), 755–761. https://doi.org/10.1002/2013GL059181

Demekhov, A. G., Trakhtengerts, V. Y., Rycroft, M., & Nunn, D. (2009). Efficiency of electron acceleration in the Earth's magnetosphere by whistler mode waves. *Geomagnetism and Aeronomy*, *49*(1), 24–29. https://doi.org/10.1134/S0016793209010034

Demekhov, A. G., Trakhtengerts, V. Y., Rycroft, M. J., & Nunn, D. (2006). Electron acceleration in the magnetosphere by whistler-mode waves of varying frequency. *Geomagnetism and Aeronomy*, *46*(6), 711–716. https://doi.org/10.1134/S0016793206060053

Drozdov, A. Y., Usanova, M. E., Hudson, M. K., Allison, H. J., & Shprits, Y. Y. (2020). The role of hiss, chorus, and EMIC waves in the modeling of the dynamics of the multi-MeV radiation belt electrons. *Journal of Geophysical Research: Space Physics*, *125*(9), e28282. https://doi.org/10.1029/2020JA028282

Engebretson, M. J., Posch, J. L., Wygant, J. R., Kletzing, C. A., Lessard, M. R., Huang, C.-L., et al. (2015). Van Allen Probes, NOAA, GOES, and ground observations of an intense EMIC wave event extending over 12 h in magnetic local time. *Journal of Geophysical Research: Space Physics*, *120*(7), 5465–5488. https://doi.org/10.1002/2015JA021227

Frey, H. U., Haerendel, G., Mende, S. B., Forrester, W. T., Immel, T. J., & Østgaard, N. (2004). Subauroral morning proton spots (SAMPS) as a result of plasmapause-ring-current interaction. *Journal of Geophysical Research*, *109*(A10), A10305. https://doi.org/10.1029/2004JA010516

Fu, X., Cowee, M. M., Friedel, R. H., Funsten, H. O., Gary, S. P., Hospodarsky, G. B., et al. (2014). Whistler anisotropy instabilities as the source of banded chorus: Van Allen Probes observations and particle-in-cell simulations. *Journal of Geophysical Research: Space Physics*, *119*(10), 8288–8298. https://doi.org/10.1002/2014JA020364

Furuya, N., Omura, Y., & Summers, D. (2008). Relativistic turning acceleration of radiation belt electrons by whistler mode chorus. *Journal of Geophysical Research*, *113*(A4), 4224. https://doi.org/10.1029/2007JA012478

Glauert, S. A., & Horne, R. B. (2005). Calculation of pitch angle and energy diffusion coefficients with the PADIE code. *Journal of Geophysical Research*, *110*(A4), 4206. https://doi.org/10.1029/2004JA010851

Grach, V. S., Artemyev, A. V., Demekhov, A. G., Zhang, X.-J., Bortnik, J., Angelopoulos, V., et al. (2022). Relativistic electron precipitation by EMIC waves: Importance of nonlinear resonant effects. *Geophysical Research Letters*, *49*(17), e99994. https://doi.org/10.1029/2022GL099994

Grach, V. S., & Demekhov, A. G. (2020). Precipitation of relativistic electrons under resonant interaction with electromagnetic ion cyclotron wave packets. *Journal of Geophysical Research: Space Physics*, *125*(2), e27358. https://doi.org/10.1029/2019JA027358

Grach, V. S., & Demekhov, A. G. (2023). Interaction of relativistic electrons with packets of the electromagnetic ion cyclotron waves of finite length and low amplitude. *Plasma Physics Reports*, *49*(7), 901–911. https://doi.org/10.1134/S1063780X23600561

Grach, V. S., Demekhov, A. G., & Larchenko, A. V. (2021). Resonant interaction of relativistic electrons with realistic electromagnetic ion-cyclotron wave packets. *Earth Planets and Space*, *73*(1), 129. https://doi.org/10.1186/s40623-021-01453-w

Hiraga, R., & Omura, Y. (2020). Acceleration mechanism of radiation belt electrons through interaction with multi-subpacket chorus waves. *Earth Planets and Space*, *72*(1), 21. https://doi.org/10.1186/s40623-020-1134-3

Horne, R. B., Kersten, T., Glauert, S. A., Meredith, N. P., Boscher, D., Sicard-Piet, A., et al. (2013). A new diffusion matrix for whistler mode chorus waves. *Journal of Geophysical Research: Space Physics*, *118*(10), 6302–6318. https://doi.org/10.1002/jgra.50594

Hsieh, Y.-K., Kubota, Y., & Omura, Y. (2020). Nonlinear evolution of radiation belt electron fluxes interacting with oblique whistler mode chorus emissions. *Journal of Geophysical Research: Space Physics*, *125*(2), e2019JA027465. https://doi.org/10.1029/2019JA027465

Hsieh, Y.-K., & Omura, Y. (2017). Nonlinear dynamics of electrons interacting with oblique whistler mode chorus in the magnetosphere. *Journal of Geophysical Research: Space Physics*, *122*(1), 675–694. https://doi.org/10.1002/2016JA023255

Hsieh, Y.-K., & Omura, Y. (2023). Precipitation rates of electrons interacting with lower-band chorus emissions in the inner magnetosphere. *Journal of Geophysical Research: Space Physics*, *128*(6), e2023JA031307. https://doi.org/10.1029/2023JA031307

Hsieh, Y.-K., Omura, Y., & Kubota, Y. (2022). Energetic electron precipitation induced by oblique whistler mode chorus emissions. *Journal of Geophysical Research: Space Physics*, *127*(1), e29583. https://doi.org/10.1029/2021JA029583

Jun, C.-W., Miyoshi, Y., Kurita, S., Yue, C., Bortnik, J., Lyons, L., et al. (2021). The characteristics of EMIC waves in the magnetosphere based on the Van Allen Probes and Arase observations. *Journal of Geophysical Research: Space Physics*, *126*(6), e29001. https://doi.org/10.1029/2020JA029001

Jun, C. W., Yue, C., Bortnik, J., Lyons, L. R., Nishimura, Y., & Kletzing, C. (2019). EMIC wave properties associated with and without injections in the inner magnetosphere. *Journal of Geophysical Research: Space Physics*, *124*(3), 2029–2045. https://doi.org/10.1029/2018JA026279

Kasahara, S., Miyoshi, Y., Yokota, S., Kasahara, Y., Matsuda, S., Kumamoto, A., et al. (2018a). Pulsating aurora from electron scattering by chorus waves. *Nature*, *554*(7692), 337–340. https://doi.org/10.1038/nature25505

Kasahara, S., Yokota, S., Mitani, T., Asamura, K., Hirahara, M., Shibano, Y., & Takashima, T. (2018b). Medium-energy particle experiments-electron analyzer (MEP-e) for the exploration of energization and radiation in geospace (ERG) mission. *Earth Planets and Space*, *70*(1), 69. https://doi.org/10.1186/s40623-018-0847-z

Katoh, Y., & Omura, Y. (2007). Relativistic particle acceleration in the process of whistler-mode chorus wave generation. *Geophysical Research Letters*, *34*(13), L13102. https://doi.org/10.1029/2007GL029758

Kersten, T., Horne, R. B., Glauert, S. A., Meredith, N. P., Fraser, B. J., & Grew, R. S. (2014). Electron losses from the radiation belts caused by EMIC waves. *Journal of Geophysical Research: Space Physics*, *119*(11), 8820–8837. https://doi.org/10.1002/2014JA020366

Le Contel, O., Roux, A., Robert, P., Coillot, C., Bouabdellah, A., de La Porte, B., et al. (2008). First results of the THEMIS Search Coil magnetometers. *Space Science Reviews*, *141*(1–4), 509–534. https://doi.org/10.1007/s11214-008-9371-y

Lee, J. H., & Angelopoulos, V. (2014). On the presence and properties of cold ions near Earth's equatorial magnetosphere. *Journal of Geophysical Research: Space Physics*, *119*(3), 1749–1770. https://doi.org/10.1002/2013JA019305

Lee, J. H., Chen, L., Angelopoulos, V., & Thorne, R. M. (2012). THEMIS observations and modeling of multiple ion species and EMIC waves: Implications for a vanishing He^{+} stop band. *Journal of Geophysical Research*, *117*(A6), A06204. https://doi.org/10.1029/2012JA017539

Li, W., & Hudson, M. K. (2019). Earth's van Allen radiation belts: From discovery to the Van Allen Probes era. *Journal of Geophysical Research: Space Physics*, *124*(11), 8319–8351. https://doi.org/10.1029/2018JA025940

Li, W., Ni, B., Thorne, R. M., Bortnik, J., Green, J. C., Kletzing, C. A., et al. (2013). Constructing the global distribution of chorus wave intensity using measurements of electrons by the POES satellites and waves by the Van Allen Probes. *Geophysical Research Letters*, *40*(17), 4526–4532. https://doi.org/10.1002/grl.50920

Lorentzen, K. R., Blake, J. B., Inan, U. S., & Bortnik, J. (2001). Observations of relativistic electron microbursts in association with VLF chorus. *Journal of Geophysical Research*, *106*(A4), 6017–6028. https://doi.org/10.1029/2000JA003018

Millan, R. M., & Thorne, R. M. (2007). Review of radiation belt relativistic electron losses. *Journal of Atmospheric and Solar-Terrestrial Physics*, *69*(3), 362–377. https://doi.org/10.1016/j.jastp.2006.06.019

Mourenas, D., Artemyev, A. V., Ma, Q., Agapitov, O. V., & Li, W. (2016). Fast dropouts of multi-MeV electrons due to combined effects of EMIC and whistler mode waves. *Geophysical Research Letters*, *43*(9), 4155–4163. https://doi.org/10.1002/2016GL068921

Ni, B., Cao, X., Zou, Z., Zhou, C., Gu, X., Bortnik, J., et al. (2015). Resonant scattering of outer zone relativistic electrons by multiband EMIC waves and resultant electron loss time scales. *Journal of Geophysical Research: Space Physics*, *120*(9), 7357–7373. https://doi.org/10.1002/2015JA021466

Ni, B., Li, W., Thorne, R. M., Bortnik, J., Green, J. C., Kletzing, C. A., et al. (2014). A novel technique to construct the global distribution of whistler mode chorus wave intensity using low-altitude POES electron data. *Journal of Geophysical Research: Space Physics*, *119*(7), 5685–5699. https://doi.org/10.1002/2014JA019935

Ni, B., Thorne, R. M., & Ma, Q. (2012). Bounce-averaged Fokker-Planck diffusion equation in non-dipolar magnetic fields with applications to the Dungey magnetosphere. *Annales Geophysicae*, *30*(4), 733–750. https://doi.org/10.5194/angeo-30-733-2012

Ni, B., Thorne, R. M., Zhang, X., Bortnik, J., Pu, Z., Xie, L., et al. (2016). Origins of the Earth's diffuse auroral precipitation. *Space Science Reviews*, *200*(1–4), 205–259. https://doi.org/10.1007/s11214-016-0234-7

Nishimura, Y., Bortnik, J., Li, W., Thorne, R. M., Ni, B., Lyons, L. R., et al. (2013). Structures of dayside whistler-mode waves deduced from conjugate diffuse aurora. *Journal of Geophysical Research: Space Physics*, *118*(2), 664–673. https://doi.org/10.1029/2012JA018242

Omura, Y., Furuya, N., & Summers, D. (2007). Relativistic turning acceleration of resonant electrons by coherent whistler mode waves in a dipole magnetic field. *Journal of Geophysical Research*, *112*(A6), 6236. https://doi.org/10.1029/2006JA012243

Omura, Y., Miyashita, Y., Yoshikawa, M., Summers, D., Hikishima, M., Ebihara, Y., & Kubota, Y. (2015). Formation process of relativistic electron flux through interaction with chorus emissions in the Earth's inner magnetosphere. *Journal of Geophysical Research: Space Physics*, *120*(11), 9545–9562. https://doi.org/10.1002/2015JA021563

Shprits, Y. Y., Drozdov, A. Y., Spasojevic, M., Kellerman, A. C., Usanova, M. E., Engebretson, M. J., et al. (2016). Wave-induced loss of ultra-relativistic electrons in the Van Allen radiation belts. *Nature Communications*, *7*(1), 12883. https://doi.org/10.1038/ncomms12883

Shprits, Y. Y., Kellerman, A., Aseev, N., Drozdov, A. Y., & Michaelis, I. (2017). Multi-MeV electron loss in the heart of the radiation belts. *Geophysical Research Letters*, *44*(3), 1204–1209. https://doi.org/10.1002/2016GL072258

Shprits, Y. Y., Subbotin, D. A., Meredith, N. P., & Elkington, S. R. (2008). Review of modeling of losses and sources of relativistic electrons in the outer radiation belt II: Local acceleration and loss. *Journal of Atmospheric and Solar-Terrestrial Physics*, *70*(14), 1694–1713. https://doi.org/10.1016/j.jastp.2008.06.014

Shumko, M., Gallardo-Lacourt, B., Halford, A. J., Blum, L. W., Liang, J., Miyoshi, Y., et al. (2022). Proton aurora and relativistic electron microbursts scattered by electromagnetic ion cyclotron waves. *Frontiers in Astronomy and Space Sciences*, *9*, 975123. https://doi.org/10.3389/fspas.2022.975123

Stix, T. H. (1962). The theory of plasma waves.

Streltsov, A. V., & Bengtson, M. T. (2020). Observations and modeling of whistler mode waves in the magnetospheric density ducts. *Journal of Geophysical Research: Space Physics*, *125*(10), e28398. https://doi.org/10.1029/2020JA028398

Summers, D. (2005). Quasi-linear diffusion coefficients for field-aligned electromagnetic waves with applications to the magnetosphere. *Journal of Geophysical Research*, *110*(A8), 8213. https://doi.org/10.1029/2005JA011159

Summers, D., Ni, B., & Meredith, N. P. (2007a). Timescales for radiation belt electron acceleration and loss due to resonant wave-particle interactions: 2. Evaluation for VLF chorus, ELF hiss, and electromagnetic ion cyclotron waves. *Journal of Geophysical Research*, *112*(A4), 4207. https://doi.org/10.1029/2006JA011993

Summers, D., Ni, B., & Meredith, N. P. (2007b). Timescales for radiation belt electron acceleration and loss due to resonant wave-particle interactions: 1. Theory. *Journal of Geophysical Research*, *112*(A4), 4206. https://doi.org/10.1029/2006JA011801

Summers, D., & Omura, Y. (2007). Ultra-relativistic acceleration of electrons in planetary magnetospheres. *Geophysical Research Letters*, *34*(24), 24205. https://doi.org/10.1029/2007GL032226

Summers, D., & Thorne, R. M. (2003). Relativistic electron pitch-angle scattering by electromagnetic ion cyclotron waves during geomagnetic storms. *Journal of Geophysical Research*, *108*(A4), 1143. https://doi.org/10.1029/2002JA009489

Summers, D., Thorne, R. M., & Xiao, F. (1998). Relativistic theory of wave-particle resonant diffusion with application to electron acceleration in the magnetosphere. *Journal of Geophysical Research*, *103*(A9), 20487–20500. https://doi.org/10.1029/98JA01740

Tao, X., Bortnik, J., Albert, J. M., Thorne, R. M., & Li, W. (2013). The importance of amplitude modulation in nonlinear interactions between electrons and large amplitude whistler waves. *Journal of Atmospheric and Solar-Terrestrial Physics*, *99*, 67–72. https://doi.org/10.1016/j.jastp.2012.05.012

Tao, X., Bortnik, J., Thorne, R. M., Albert, J. M., & Li, W. (2012). Effects of amplitude modulation on nonlinear interactions between electrons and chorus waves. *Geophysical Research Letters*, *39*(6), 6102. https://doi.org/10.1029/2012GL051202

Tao, X., Thorne, R. M., Li, W., Ni, B., Meredith, N. P., & Horne, R. B. (2011). Evolution of electron pitch angle distributions following injection from the plasma sheet. *Journal of Geophysical Research*, *116*(A4), A04229. https://doi.org/10.1029/2010JA016245

Thorne, R. M., Bortnik, J., Li, W., & Ma, Q. (2021). Wave–particle interactions in the Earth's magnetosphere. In *Magnetospheres in the solar system* (pp. 93–108). American Geophysical Union (AGU). https://doi.org/10.1002/9781119815624.ch6

Tsai, E., Artemyev, A., Zhang, X.-J., & Angelopoulos, V. (2022). Relativistic electron precipitation driven by nonlinear resonance with whistler-mode waves. *Journal of Geophysical Research: Space Physics*, *127*(5), e30338. https://doi.org/10.1029/2022JA030338

Usanova, M. E., Drozdov, A., Orlova, K., Mann, I. R., Shprits, Y., Robertson, M. T., et al. (2014). Effect of EMIC waves on relativistic and ultrarelativistic electron populations: Ground-based and Van Allen Probes observations. *Geophysical Research Letters*, *41*(5), 1375–1381. https://doi.org/10.1002/2013GL059024

Vainchtein, D., Zhang, X. J., Artemyev, A. V., Mourenas, D., Angelopoulos, V., & Thorne, R. M. (2018). Evolution of electron distribution driven by nonlinear resonances with intense field-aligned chorus waves. *Journal of Geophysical Research: Space Physics*, *123*(10), 8149–8169. https://doi.org/10.1029/2018JA025654

Yahnin, A. G., Yahnina, T. A., Raita, T., & Manninen, J. (2017). Ground pulsation magnetometer observations conjugated with relativistic electron precipitation. *Journal of Geophysical Research: Space Physics*, *122*(9), 9169–9182. https://doi.org/10.1002/2017JA024249

Yahnin, A. G., Yahnina, T. A., Semenova, N. V., Gvozdevsky, B. B., & Pashin, A. B. (2016). Relativistic electron precipitation as seen by NOAA POES. *Journal of Geophysical Research: Space Physics*, *121*(9), 8286–8299. https://doi.org/10.1002/2016JA022765

Zhang, X. J., Agapitov, O., Artemyev, A. V., Mourenas, D., Angelopoulos, V., Kurth, W. S., et al. (2020a). Phase decoherence within intense chorus wave packets constrains the efficiency of nonlinear resonant electron acceleration. *Geophysical Research Letters*, *47*(20), e89807. https://doi.org/10.1029/2020GL089807

Zhang, X. J., Mourenas, D., Artemyev, A. V., Angelopoulos, V., Kurth, W. S., Kletzing, C. A., & Hospodarsky, G. B. (2020b). Rapid frequency variations within intense chorus wave packets. *Geophysical Research Letters*, *47*(15), e88853. https://doi.org/10.1029/2020GL088853

Zhang, X.-J., Angelopoulos, V., Artemyev, A., Mourenas, D., Agapitov, O., Tsai, E., & Wilkins, C. (2023). Temporal scales of electron precipitation driven by whistler-mode waves. *Journal of Geophysical Research: Space Physics*, *128*(1), e2022JA031087. https://doi.org/10.1029/2022JA031087

Zhang, X.-J., Angelopoulos, V., Mourenas, D., Artemyev, A., Tsai, E., & Wilkins, C. (2022). Characteristics of electron microburst precipitation based on high-resolution ELFIN measurements. *Journal of Geophysical Research: Space Physics*, *127*(5), e30509. https://doi.org/10.1029/2022JA030509

Zhang, X. J., Demekhov, A. G., Katoh, Y., Nunn, D., Tao, X., Mourenas, D., et al. (2021). Fine structure of chorus wave packets: Comparison between observations and wave generation models. *Journal of Geophysical Research: Space Physics*, *126*(8), e29330. https://doi.org/10.1029/2021JA029330

Zhang, X. J., Mourenas, D., Artemyev, A. V., Angelopoulos, V., Bortnik, J., Thorne, R. M., et al. (2019). Nonlinear electron interaction with intense chorus waves: Statistics of occurrence rates. *Geophysical Research Letters*, *46*(13), 7182–7190. https://doi.org/10.1029/2019GL083833

Zhang, X.-J., Mourenas, D., Artemyev, A. V., Angelopoulos, V., & Thorne, R. M. (2017). Contemporaneous EMIC and whistler mode waves: Observations and consequences for MeV electron loss. *Geophysical Research Letters*, *44*(16), 8113–8121. https://doi.org/10.1002/2017GL073886

Zheng, L., Chen, L., & Zhu, H. (2019). Modeling energetic electron nonlinear wave-particle interactions with electromagnetic ion cyclotron waves. *Journal of Geophysical Research: Space Physics*, *124*(5), 3436–3453. https://doi.org/10.1029/2018JA026156